Geophysical Research Letters

RESEARCH LETTER
10.1029/2022GL100378

Key Points:

- Last Glacial Maximum (LGM) experiments indicate that both warmer and colder sea surface temperature (SSTs) are inconsistent with glacial land surface temperature (LST) reconstructions
- A higher reconstruction data coverage is needed for low-elevation locations, particularly in South America and Australia
- Evaluation of climate models is still a challenge by using reconstructed LST and SST for the LGM

Correspondence to:
S. Krätschmer,
stephan.kraetschmer@awi.de

Citation:
Krätschmer, S., Cauquoin, A., Lohmann, G., & Werner, M. (2022). A modeling perspective on the lingering glacial sea surface temperature conundrum. *Geophysical Research Letters*, *49*, e2022GL100378. https://doi.org/10.1029/2022GL100378

Received 8 JUL 2022
Accepted 22 NOV 2022

Author Contributions:
Conceptualization: G. Lohmann, M. Werner
Formal analysis: S. Krätschmer
Investigation: S. Krätschmer
Methodology: S. Krätschmer, G. Lohmann, M. Werner
Project Administration: M. Werner
Resources: A. Cauquoin
Software: A. Cauquoin
Supervision: G. Lohmann, M. Werner
Validation: S. Krätschmer, G. Lohmann, M. Werner
Visualization: S. Krätschmer
Writing – original draft: S. Krätschmer
Writing – review & editing: S. Krätschmer, A. Cauquoin, G. Lohmann, M. Werner

A Modeling Perspective on the Lingering Glacial Sea Surface Temperature Conundrum

S. Krätschmer[1], A. Cauquoin[2], G. Lohmann[1,3], and M. Werner[1]

[1]Alfred Wegener Institute, Helmholtz Centre for Polar and Marine Research, Bremerhaven, Germany, [2]Institute of Industrial Science (IIS), The University of Tokyo, Kashiwa, Japan, [3]Physics Department, University of Bremen, Bremen, Germany

Abstract The strong cooling during the Last Glacial Maximum (LGM, 21 ka BP) provides a rigorous test of climate models' ability to simulate past and future climate changes. We force an atmospheric general circulation model with two recent global LGM sea surface temperature (SST) reconstructions, one suggesting a weak and the other a more pronounced cooling, and compare the simulated land surface temperatures (LSTs) to reconstructed data. Our results do not confirm either SST reconstruction. The cold SST data set leads to good agreement between simulated and observed LSTs at low latitudes, but is systematically too cold at mid-latitudes. The opposite is true for the warm SST data set. Differences between the simulated LSTs are caused by varying land surface albedos, which is lower for the warmer SST reconstruction. The inconsistency between reconstructed and simulated climate points to a potentially significant bias in the proxy reconstructions and/or the climate sensitivity of current climate models.

Plain Language Summary The global temperatures during the Last Glacial Maximum at around 21 ka BP were much lower than at present, mainly caused by large ice sheets covering large parts of North America and Europe as well as a strong reduction in atmospheric greenhouse gas concentration. A quantification of the land and sea surface cooling is necessary to understand the response of the climate system to such forcing, providing a constraint of models for future climate changes. However, recent sea surface temperature (SST) data sets still show discrepancies in the suggested cooling due to different reconstruction methods. We use both a comparably warm and a rather cold SST data set for our model simulations and compare the results to recent land surface temperature (LST) reconstructions in order to assess which SST data set leads to a higher accordance. The results are ambiguous. The warmer SST data set results in too warm simulated LST at low latitudes, but a good accordance at mid-latitudes. On the other hand, the colder SST data set yields a good accordance for low latitudes, but simulates too cold LST at mid-latitudes. This model-data inconsistency demands a critical reexamination of both proxy data and models.

1. Introduction

The Last Glacial Maximum (LGM, 21 ka BP) was characterized by a climate much colder than at present, mainly due to a strong reduction in atmospheric greenhouse gas concentrations and increased albedo as a consequence of enlarged ice cover in high latitudes (Schneider von Deimling et al., 2006). Since the surface temperature differs between the LGM and the pre-industrial period (PI, 1850–1880 CE), the LGM offers an opportunity to derive independent estimates of Earth's equilibrium climate sensitivity (Hoffert & Covey, 1992; Schmittner et al., 2011). This effort requires proper data-model comparisons and correct reconstructions of surface temperatures. The first global reconstruction of glacial sea surface temperatures (SST) was performed in the late 1970s in the scope of the Climate: Long range Investigation, Mapping, and Prediction (CLIMAP) project (CLIMAP Project Members, 1976), and the question concerning the glacial temperature drop remains controversial. The CLIMAP reconstructions suggest globally a comparably weak cooling by (3.0 ± 0.6)°C during the LGM, which results in a climate sensitivity of (2.0 ± 0.5)°C (Hoffert & Covey, 1992). This value is at the lower end of the 1.8°C–5.6°C interval (with a mean of (3.7 ± 1.1)°C) derived from the latest-generation climate model ensemble used in the scope of the sixth Coupled Model Intercomparison Project (Meehl et al., 2020). Based on the transfer function method using data from three planktonic groups preserved in deep sea sediments, the average cooling of the tropical SSTs is proposed to be only around 1°C–2°C, with even a warming in some subtropical gyres. While climate models are generally able to reproduce the changes in SST during the LGM averaged over the tropical ocean basin suggested by data (Braconnot et al., 2007), several complex models were not able to reproduce this particular feature (Waelbroeck et al., 2009). This indicates that either models are not yet able to capture important processes

in the climate system, or that some of the applied methods to reconstruct the temperature have a systematic bias. However, the importance of a proper tropical SST reconstruction during the LGM is emphasized by studies showing that the tropics have a substantial influence on the temperature and precipitation in the mid-latitudes (Lohmann & Lorenz, 2000), and that the climate sensitivity depends significantly on the tropical temperatures, resulting in a higher sensitivity in case of cooler LGM SSTs (Hargreaves et al., 2012; Yin & Battisti, 2001). Mix et al. (1999) suggested that the problem on the data side might be caused by the utilization of so-called no-analog assemblages, that is, species that do not exist today anymore and therefore are hard to interpret, for example, certain tropical Pacific foraminifera found in marine sediment cores.

A recent global SST reconstruction for the LGM is provided by Tierney et al. (2020). The authors use a data assimilation technique and cross-validate their results by simulations with an isotope-enabled climate model. Their data consist solely of geochemical proxies ($\mathbf{U}^{\mathbf{K'}}_{37}$ from alkenones, TEX_{86} based on archeal isoprenoid tetraethers, Mg/Ca of planktic foraminifera and the water isotope $\delta^{18}O$), taking into account seasonal bias and general proxy uncertainties. The approach excludes marine and terrestrial microfossils completely to avoid the no-analogs problem and the lack of Bayesian proxy-system models required in the scope of the data assimilation process. The final reconstruction suggests a mean global surface temperature reduction of −6.1°C, with a 95% probability for the interval from −5.7°C to −6.5°C. However, the authors emphasize that their result has no overlap with some other reconstructions, for example, the *Glacial Ocean Map* (GLOMAP), a global climatology of the ocean surface during the LGM mapped on a regular grid provided by Paul et al. (2021). Their study is based upon floral and faunal assemblages and several sea-ice reconstructions from the Multiproxy Approach for the Reconstruction of the Glacial Ocean Surface (MARGO, Waelbroeck et al. (2009)) project because those have the best spatial coverage available and enable potentially a seasonal reconstruction. The GLOMAP results suggest a global ocean cooling by (-1.7 ± 0.1)°C and a tropical ocean cooling by (-1.2 ± 0.3)°C for the LGM, but the authors state that their values might be too warm by 0.5°C–1°C due to the effects of a heterogenous spatial sampling and uncertainties concerning the response of fossil foraminifera to changes in seasonality and the thermal structure of the upper ocean layer.

GLOMAP and Tierney et al. SSTs provide constraints with a large range of possible conditions in between. They have been chosen in the scope of the Paleoclimate Modeling Intercomparison Project—Phase 4 (PMIP4) to compare simulation results of coupled model setups to observational data (Kageyama et al., 2021). Other LGM SST reconstructions, for example, by Annan and Hargreaves (2013) or Kurahashi-Nakamura et al. (2017), suggest a global cooling that lays between GLOMAP and Tierney et al. SSTs (Figure 7 in Paul et al. (2021)). However, PMIP4 shows clearly that coupled models, that is, Atmosphere-Ocean General Circulation Models, result in too warm simulated land surface temperatures (LSTs) (Figure 10e in Kageyama et al. (2021)). Simpler experimental designs according to the Atmospheric Model Intercomparison Project (AMIP) (Gates et al., 1999), where boundary conditions are prescribed in form of SSTs and SIC, have shown that the simulated climate evolves closer to observational data. This is caused by the reduced degrees of freedom and uncertainty that is introduced by an additional ocean model.

In this study, we use the two SST reconstructions provided by Tierney et al. (2020) and Paul et al. (2021) to force an Atmospheric General Circulation Model (AGCM) including an aerosol model. We assess our results by comparing the simulated LST difference between LGM and PI to reconstructed data based on noble gases in groundwater provided by Seltzer et al. (2021), who suggest that the low-to-mid latitude land surface during the LGM cooled by (5.8 ± 0.6)°C and stated that their LSTs are consistent with the SSTs by Tierney et al. (2020).

2. Model and Experimental Setup

For our study, we use the AGCM ECHAM6.3 coupled to the aerosol model HAM2.3 (Stevens et al., 2013; Stier et al., 2005). In the following, we will give a brief overview on the model. A more comprehensive description and detailed evaluation for present climate can be found in Tegen et al. (2019) and Neubauer et al. (2019).

2.1. The Global Aerosol-Climate Model ECHAM6.3-HAM2.3

ECHAM6.3 (subversion 6.3.02) is the latest release of ECHAM, which was mainly developed at the Max-Planck Institute for Meteorology in Hamburg. The adiabatic core of the model solves the primitive equations for the variables vorticity, divergence, temperature, and surface pressure. The horizontal discretization is based on

a spectral-transform method, which applies a triangular truncation with a finite number of modes (e.g., T63) (Simmons et al., 1989). The vertical is discretized on a Lorenz grid up to a height of approx. 80 km with either 47 or 95 layers. Implemented numerical schemes are inherently conservative in terms of mass, energy, and momentum (Lin & Rood, 1996; Simmons & Jiabin, 1991).

The physics package, which accounts for diabatic sub-grid scale processes, includes parameterizations for boundary layer turbulence (Brinkop & Roeckner, 1995), several types of convection with a preference for deep convection and momentum transfer due to gravity waves (Lott, 1999). Sub-grid scale cloudiness is parameterized based on the relative humidity according to Sundqvist et al. (1989). The coupling to the aerosol model HAM2.3 allows for an explicit calculation of cloud droplet numbers, and the transport of cloud water and ice is prognostically calculated (Lohmann & Roeckner, 1996). In order to calculate the radiative transfer, the spectrum of the incoming and outgoing electromagnetic radiation is divided into 14 shortwave and 16 longwave bands, and for all bands lookup-tables are used to determine the absorption by greenhouse gases. Optical properties of clouds are calculated based on Mie theory. A integrated land surface and vegetation model (JSBACH, Reick et al. (2013)) allows for the consideration of dynamic vegetation, taking into account several types of bare soil and 12 different plant functional types combined with a five-layer soil hydrology scheme (Hagemann & Stacke, 2015). Albedo is likewise calculated dynamically by JSBACH with a scheme described in detail by Otto et al. (2011). The aerosol model HAM2.3 calculates the aerosol dynamics of the five aerosol species sea spray, mineral dust, sulfate, black, and organic carbon based on a general coagulation equation and considers size-dependent processes like emission and deposition, inter- and intra-modal coagulation, particle growth, and mode-transfer between insoluble and soluble modes (Neubauer et al., 2019; Stier et al., 2005; Tegen et al., 2019).

2.2. Experiments and Experimental Setup

We perform simulations for PI (1850–1879 CE) and LGM climate conditions with the horizontal spatial resolution T63, corresponding to 1.875° × 1.875°, and 47 vertical layers. For PI, we initialize a cold start with a spin-up time of 10 years, and for the LGM we initialize the simulations by restart files, which represent a dynamic equilibrium of the model obtained after several hundred simulation years. More details on the setup can be found in Krätschmer et al. (2022). We run each simulation for 50 years, and our assessment period covers the final 30 years. The SST and sea ice boundary conditions we prescribe in our atmosphere-only setup for PI are monthly resolved values averaged for the years 1870–1899 and stem from the Program for Climate Model Diagnosis and Intercomparison based on the latest AMIP II data set (Durack & Taylor, 2019). For the LGM, we use the reconstructions from Tierney et al. (2020) ($LGM_{Tierney}$) and GLOMAP (LGM_{GLOMAP}, Paul et al. (2021)). Since Tierney et al. (2020) do not provide a sea ice reconstruction, we use the one from GLOMAP to keep the LGM experiment setup as similar as possible in order to investigate the sole influence of the SST. Anthropogenic emissions of aerosols and aerosol precursor are only of importance for PI, and here we prescribe monthly resolved input files based on the Atmospheric Chemistry and Climate Model Intercomparison Project data set (Lamarque et al., 2010). The orbital parameters, greenhouse gas concentrations and the glacier mask (GLAC-1D, Tarasov et al. (2012)) for the LGM runs are set in accordance with the PMIP4 experimental design (Kageyama et al., 2017).

3. Results and Discussion

Our results focus solely on the simulated surface temperature difference ΔT between LGM and PI for both prescribed sea surface temperature reconstructions.

3.1. Globally and Zonally Simulated Surface Temperature Difference for GLOMAP and Tierney SST

Figure 1 shows the zonally averaged sea and LST for PI, (Figure 1a) LGM_{GLOMAP} and (Figure 1b) $LGM_{Tierney}$. Since we prescribe in both experiments the same glacier mask and sea ice reconstruction, there is only little difference for the mid/high-latitudes. The most remarkable differences occur particularly in the latitudes 45°N–45°S. Globally, the experiments result in a cooling of −4.08°C (LGM_{GLOMAP}), respectively, −6.12°C ($LGM_{Tierney}$) of the surface temperature. In LGM_{GLOMAP}, the total cooling in the low latitudes (30°N–30°S) averages to −1.28°C, with a more pronounced cooling of the land surface (−2.07°C) than the sea surface (−0.98°C). A similar anomaly is also found if one focuses on the tropics (23.5°N–23.5°S), with a total cooling of −1.22°C. However, even though the considered tropics region has less influence from the mid/high-latitudes, the sea surface temperature

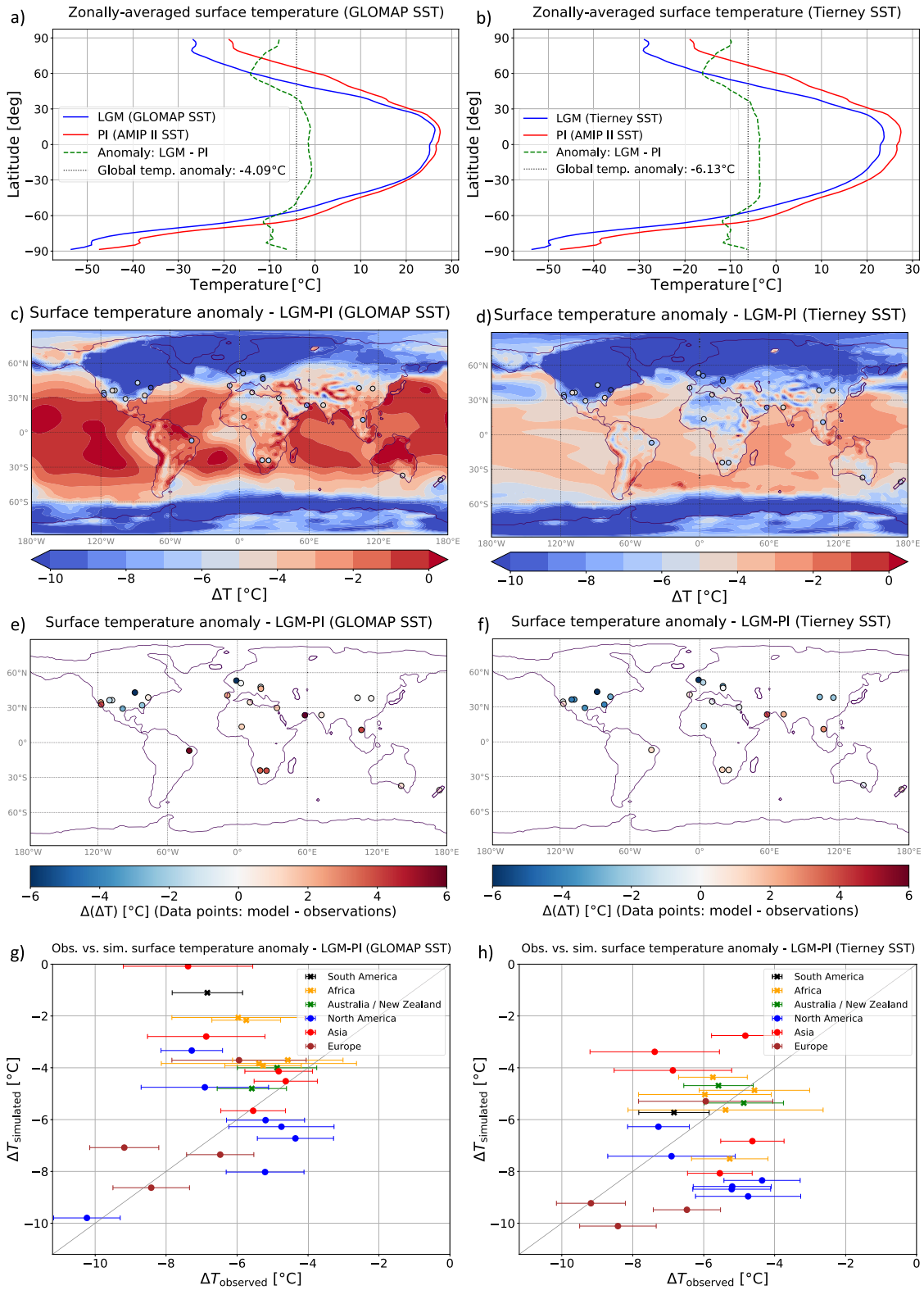

Figure 1.

Table 1
Globally and Regionally Simulated Cooling Between Last Glacial Maximum (LGM) and Pre-Industrial Period Averaged Over the Total, Sea and Land Surface for LGM_{GLOMAP} and $LGM_{Tierney}$

$\Delta T_{LGM\text{-}PI}$ (°C)		LGM_{GLOMAP}	$LGM_{Tierney}$
Global		−4.08	−6.12
Low latitudes (30°N–30°S)	Total	−1.28	−3.80
	Sea surface	−0.98	−3.50
	Land surface	−2.07	−4.59
Tropics (23.5°N–23.5°S)	Total	−1.22	−3.71
	Sea surface	−1.00	−3.46
	Land surface	−1.83	−4.43

cooling is even slightly stronger (−1.0°C) than the average over the low latitudes between 30°N and 30°S. This difference is caused by the warm pools in the subtropical gyres, which are less extensive closer to the equator (see Figure 1c). $LGM_{Tierney}$, on the other hand, results in a much stronger total cooling than LGM_{GLOMAP}, both in the low latitudes (−3.80°C) and also in the tropics (−3.71°C). Likewise, the land surface cooling by −4.59°C (−4.43°C) at low latitudes (tropics) is more pronounced than the sea surface cooling of −3.50°C (−3.46°C). All values are summarized in Table 1.

Both experiments, LGM_{GLOMAP} and $LGM_{Tierney}$, suggest a stronger cooling during the LGM than the (3.0 ± 0.6)°C proposed by the CLIMAP reconstruction. The mean cooling simulated in the high northern latitudes by approx. 10°C, which is caused by the ice sheets covering large parts of northern Europe and North America, is in good accordance with other modeling studies (Cao et al., 2019; Romanova et al., 2006). Similarly, a comparably lower cooling simulated over Antarctica is supported by reconstructions (e.g., Buizert et al. (2019)). The zonal and regional differences are discussed in more detail Section 3.2 with regard to the available data.

3.2. Comparison of the Simulated LST Anomaly to Reconstructed Data

Figure 1 shows the comparison between the reconstructed LST by Seltzer et al. (2021) and our simulation results for LGM_{GLOMAP} and $LGM_{Tierney}$ in form of (Figures 1c–1f) global maps and (Figures 1g and 1h) scatterplots.

The most remarkable differences in the simulated surface temperature anomaly occur in the low latitudes (Figures 1c–1f). LGM_{GLOMAP} shows a comparably weak cooling in basically all low-latitude regions of the Pacific Ocean of less than −1°C, and also exhibit the controversial warming in subtropical gyres in the Pacific and the Atlantic Ocean. The weak low-latitude sea surface cooling leads to simulated LSTs in the same range that are all too warm as compared to the reconstructions by Seltzer et al. (Figures 1e and 1g). In this study, we have grouped locations in regions within or very close to the low latitudes, that is, South America, Africa, and Australia/New Zealand, and compare them to regions that are rather located in the mid-latitudes, like North America, Europe, and Asia. The entire neotropical realm is only covered by one observation in the north-eastern part of South America. In contrast to $LGM_{Tierney}$, LGM_{GLOMAP} clearly underestimates the cooling here. This is not surprising considering that we found in a previous study (Krätschmer et al., 2022), in which we prescribed the comparably warm GLAMAP SST (predecessor of GLOMAP, Paul and Schäfer-Neth (2003)), that the JSBACH vegetation model simulates a desert in this region due to high temperatures and strongly reduced precipitation. However, the drier climate simulated in this region is also supported by pollen and plant macrofossil data, which show that the plant-available moisture was strongly reduced during the LGM compared to present day (Farrera et al., 1999). The study by Farrera et al. (1999) also proposes a cooling by −5°C to −6°C for neotropical sites, which is much stronger than supported by our LGM_{GLOMAP} experiment, but in good agreement with results of our $LGM_{Tierney}$ experiment (Figures 1f and 1h). However, the authors state that data from West and South Pacific sites suggest only a reduced LGM sea level cooling by −1°C. This indicates that the CLIMAP-like SST anomalies, that is, the warmer pools in the subtropical gyres, might actually be realistic and thus this data also partly support the GLOMAP SST reconstructions. The LST reconstruction from Vietnam provided by Seltzer et al. (2021) is colder than our simulation results for both SST reconstructions, and closer to $LGM_{Tierney}$. However, low-elevation records from Indonesia and Papua New Guinea provided by Farrera et al. (1999) suggest again only a weak cooling by −1°C to −2°C, supporting both LGM_{GLOMAP} and $LGM_{Tierney}$. Similarly, LGM temperature changes in Australia and New Zealand are in both experiments in accordance with the two observational records, but the low

Figure 1. Zonally averaged surface temperatures during the Last Glacial Maximum (LGM) for both (a) LGM_{GLOMAP} and (b) $LGM_{Tierney}$ compared to pre-industrial period (PI) (Atmospheric Model Intercomparison Project II sea surface temperature). Comparison between the simulated surface temperature anomaly (LGM—PI) for (c, e, and g) LGM_{GLOMAP} and (d, f, and h) $LGM_{Tierney}$ and reconstructed values based on noble gas concentrations in groundwater provided by Seltzer et al. (2021). For easier readability, the difference between simulated and measured surface temperature anomaly $\Delta(\Delta T)$ is additionally shown for the data points in panels (c and d), indicating that the simulated temperature anomaly is higher ($\Delta(\Delta T) > 0$) or lower ($\Delta(\Delta T) < 0$) than suggested by the reconstructions. Data points in the scatterplots (g and h) are plotted with their reconstruction uncertainty given by Seltzer et al. (2021) and grouped into regions at low latitudes (pluses, South America, Africa, Australia/New Zealand) and regions predominantly in the mid-latitudes (circles, North America, Europe, Asia).

data coverage does not allow for any further insights. The agreement between simulation results and observations for the African continent is generally good for $LGM_{Tierney}$ (Figures 1f and 1h). LGM_{GLOMAP}, on the other hand, simulated systematically too warm LSTs here, especially in South Africa (Figure 1e). A TEX_{86} proxy record from Lake Malawi in East Africa indicates a 3.5°C cooling during the LGM, which is also in better accordance with $LGM_{Tierney}$ (Powers et al., 2005). At the data sites in North America and Europe as well as two regions in mid-latitude Asia, $LGM_{Tierney}$ result systematically in too cold LSTs (Figures 1f and 1h). Our simulation results obtained in LGM_{GLOMAP} are, on the other hand, in better accordance with the reconstructed data, particularly in some locations in western North America. Here, the simulated lower cooling compared to $LGM_{Tierney}$ might be caused by changes in the atmospheric circulation due to the Laurentide ice sheets. Bartlein et al. (2011) suggested that a potential warming in Alaska during the LGM might have been caused by warm air advectively transported from the south. Romanova et al. (2006) found that the changes of the orography and albedo caused by the Laurentide Ice Sheet induce strong temperature changes of about 16°C north of 30°N, and much smaller changes elsewhere. These temperature changes are found to be non-linearly related to ice sheet height with regional heterogeneities (Meyer et al., 2017; Romanova et al., 2006; Wang et al., 2021).

In general, LGM_{GLOMAP} results in a simulated mean LST difference between LGM and PI of −5.76 K (standard deviation (SD) = 4.38 K, mean absolute difference to Seltzer et al. data (MAD) = 2.84 K), which is closer to the data-based value of −6.12 K (SD = 1.43 K) provided by Seltzer et al. (2021) than the simulated −7.81 K (SD = 4.50 K, MAD = 2.82 K) in $LGM_{Tierney}$. At first, it seems that both simulations are equally in agreement with the observations overall. However, Figures 1g and 1h show that for mid-latitude regions, that is, North America, Asia, and Europe, 7 out of 16 data points are in agreement with the reconstructed data for LGM_{GLOMAP} within the reconstruction accuracy, but only 2/16 for $LGM_{Tierney}$. For low latitudes, that is, South America, Africa, and Australia/New Zealand, 4 out of 8 data points are in agreement with the observational data for both experiments. However, looking at the cluster of data points, it becomes obvious that values from $LGM_{Tierney}$ are much closer to the observations. For instance, the data point from South America is not in agreement with either simulation, however, it is obvious that the discrepancy is substantially smaller for $LGM_{Tierney}$. The same applies to several data points from Africa. Conversely, the discrepancy for North American and European data points is much larger in $LGM_{Tierney}$ than in LGM_{GLOMAP}.

3.3. Physical Mechanisms Causing Simulated Changes in LSTs for Different SSTs

Figure 2a shows the zonally averaged TOA radiation balance (incoming minus outgoing radiation). Although the incoming radiation is identical in both LGM experiments, the Earth takes up more energy between 40°N and 40°S in $LGM_{Tierney}$. This is caused by the generally colder temperatures due to the colder SSTs, resulting in less outgoing longwave radiation which scales with the fourth power of the temperature according to the Stefan-Boltzmann law.

The surface albedo anomaly (LGM_{GLOMAP} minus $LGM_{Tierney}$) is shown in Figure 2b. For LGM_{GLOMAP}, the albedo is reduced in large parts of North America, Europe, and Asia compared to $LGM_{Tierney}$. This is caused by slightly increased vegetation cover in mid-latitudes and warmer temperatures over snowy/icy surfaces, which result both in lower albedo (Otto et al., 2011). The warmer (air) temperatures are a consequence of the warmer SSTs. Reduced albedo implies a higher absorption of radiation by the surface, which in turn increases the LST. This pattern can be found in the maps for the TOA and surface radiation anomaly (Figures 2c and 2d), which in turn is in good agreement with the surface temperature anomaly maps in our manuscript (Figures 2a and 2b). Differences in energy uptake between TOA (Figure 2c) and surface (Figure 2d) can be traced back to atmospheric processes. The globally higher atmospheric temperatures in LGM_{GLOMAP} result in increased atmospheric water vapor concentration, which affects cloudiness (planetary albedo) on the one hand and the absorption of longwave radiation (absorptivity/emissivity) on the other hand. As can be seen in Figures 2c and 2d, these processes play a crucial role in the tropics, particularly in Southeast Asia and the northeastern part of South America.

In order to investigate quantitatively the individual contributions of simulated changes in emissivity and albedo to changes in the globally averaged temperature between LGM and PI, we determine these parameters based on our model results and compare it to the temperature given by a simple 0-dimensional energy balance model (EBM, see Equation 3 in Lohmann (2020)) after inserting our model-derived values. The results are shown in Figure 2 for LGM_{GLOMAP} (Figure 2e) and $LGM_{Tierney}$ (Figure 2f). Although the EBM is generally colder than the GCM for each scenario, it reproduces the stronger overall cooling (LGM minus PI, see Table 1) in $LGM_{Tierney}$ (−6.57 K)

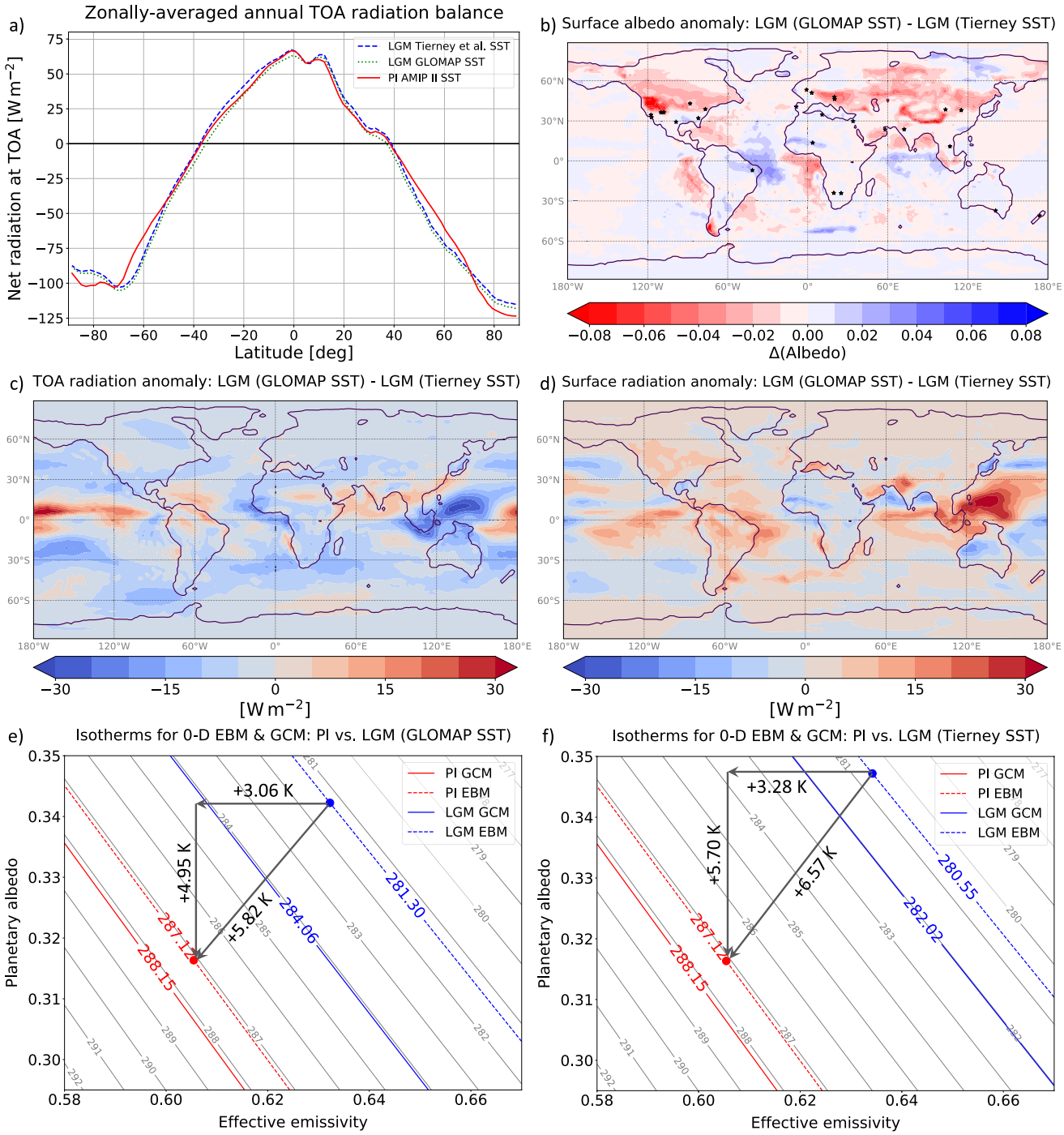

Figure 2. Shown are the zonally averaged TOA radiation balance for pre-industrial period (PI) and both Last Glacial Maximum (LGM) experiments (a), the surface albedo anomaly (LGM_{GLOMAP} minus $LGM_{Tierney}$) (b), and maps for the TOA and surface radiation anomalies (c and d). Differences in sea water albedo between LGM_{GLOMAP} and $LGM_{Tierney}$ can be traced back to the parameterization scheme, which depends on direct and diffuse downward radiation in the visible and near-infrared spectrum. Additionally, the comparison between our simulation results and results from a simple 0-dimensional energy balance model in terms of changes in globally averaged temperature, effective emissivity and planetary albedo is shown for LGM_{GLOMAP} (e) and $LGM_{Tierney}$ (f) along with the values for PI. Values of contour lines are given in Kelvin. Gray lines represent isotherms in increments of 1 K and are shown for improved readability. Black arrows and numbers indicate individual contributions from changes in emissivity and albedo to the temperature difference between LGM and PI.

compared to LGM_{GLOMAP} (−5.82 K) correctly. The EBM also indicates that cooling due to changes in effective emissivity is similar for LGM_{GLOMAP} (−3.06 K) and $LGM_{Tierney}$ (−3.28 K). Additionally, it shows that the global temperature discrepancy is predominantly caused by changes in planetary albedo, which results in a stronger cooling in $LGM_{Tierney}$ (−5.70 K) compared to LGM_{GLOMAP} (−4.95 K). This finding is in agreement with results shown in Figures 2b and 2d, which suggest that decreased albedo in LGM_{GLOMAP} and the resulting enhanced land surface energy uptake is mainly responsible for differences in the LSTs in our simulations.

4. Conclusions

The comparison of our simulation results using both Tierney et al. and GLOMAP SSTs gives no clear indication which reconstruction results in overall better-fitting LSTs. Differences in simulated LSTs between LGM_{GLOMAP} and $LGM_{Tierney}$, particularly in the mid-latitudes, can be traced back to changes in land surface albedo due to variations in the vegetation cover and a temperature-dependent albedo of snowy/icy surfaces. From the data side, a higher low-elevation coverage obtained by using the same reconstruction method in some regions, particularly the neotropical realm and Australia/New Zealand, would be desirable.

Although the LGM is one of the most frequently simulated time slices in paleoclimate modeling and belongs to the standard PMIP model experiments (Braconnot et al., 2012; Kageyama et al., 2021), a consistent view of the marine and terrestrial reconstructions is still lacking. In order to estimate the Earth's climate sensitivity based on simulations, the models have to represent several feedback mechanisms in the climate system correctly. In the tropics, which are particularly important for the global climate due their large spatial extent, relevant mechanisms include the cloud feedback and the water vapor—lapse rate feedback (Bony et al., 2006). Since there is still conflicting evidence on the LGM lapse rate change (Banerjee et al., 2022; Loomis et al., 2017), it represents another important target for model-data comparison. As pointed out by Seltzer et al. (2021), the lapse rate is critical for a comparison between simulated and reconstructed SSTs and LSTs, respectively, since the 130 m lower sea level might also lead to an additional temperature change. Another source of uncertainty are the model resolution and the parameterization of physical processes on the sub-grid scale. Model results with increased grid resolution demonstrate more realistic climate simulations due to the higher number and improved representation of climate processes and phenomena in the model (Lohmann et al., 2021; Roeckner et al., 2006). Modeling studies also indicate a substantial influence of variations in soil albedo on simulated LSTs, which might result in an additional global cooling by 1.07°C during the LGM (Stärz et al., 2016).

Based on our study, we propose an AMIP style experimental design for the LGM to the community and strongly encourage other research groups to force their AGCMs likewise with the two different SST reconstructions used here. The comparison of simulation results obtained by different models will minimize individual model biases introduced by differences in the parameterization schemes, complexity of the models and the grid resolution. The combined effort might lead to an improved understanding of glacial surface temperatures.

Conflict of Interest

The authors declare no conflicts of interest relevant to this study.

Acknowledgments
The work was supported by the research topic "Ocean and Cryosphere under climate change" in the program "Changing Earth—Sustaining our future" of the Helmholtz Society. We acknowledge support by the Open Access Publication Funds of Alfred Wegener Institute Helmholtz Centre for Polar and Marine Research. We thank the Center for Climate Systems Modeling (C2SM) at ETH Zurich for hosting and providing the ECHAM-HAMMOZ model code. We acknowledge a discussion with Werner Aeschbach. Finally, we would like to thank the editor Sarah Feakins and two anonymous reviewers for their helpful input on our manuscript.

Data Availability Statement

The ECHAM-HAMMOZ model is developed by a consortium composed of ETH Zurich, Max Planck Institute for Meteorology in Hamburg, Forschungszentrum Jülich, University of Oxford, and the Finnish Meteorological Institute and managed by the Center for Climate Systems Modeling (C2SM) at ETH Zurich. The code and all required input files can be obtained from https://redmine.hammoz.ethz.ch/projects/hammoz/wiki/01_Hitchhikers_guide_to_hammoz after signing a license agreement.

References

Annan, J. D., & Hargreaves, J. C. (2013). A new global reconstruction of temperature changes at the Last Glacial Maximum. *Climate of the Past*, *9*(1), 367–376. https://doi.org/10.5194/cp-9-367-2013

Banerjee, A., Yeung, L. Y., Murray, L. T., Tie, X., Tierney, J. E., & Legrande, A. N. (2022). Clumped-isotope constraint on upper-tropospheric cooling during the Last Glacial Maximum. *AGU Advances*, *3*(4), e2022AV000688. https://doi.org/10.1029/2022AV000688

Bartlein, P. J., Harrison, S. P., Brewer, S., Connor, S., Davis, B. A. S., Gajewski, K., et al. (2011). Pollen-based continental climate reconstructions at 6 and 21 ka: A global synthesis. *Climate Dynamics*, *37*(3), 775–802. https://doi.org/10.1007/s00382-010-0904-1

Bony, S., Colman, R., Kattsov, V., Allan, R., Bretherton, C., Dufresne, J., et al. (2006). How well do we understand and evaluate climate change feedback processes? *Journal of Climate*, *3445*(15), 3445–3482. https://doi.org/10.1175/JCLI3819.1

Braconnot, P., Harrison, S. P., Kageyama, M., Bartlein, P. J., Masson-Delmotte, V., Abe-Ouchi, A., et al. (2012). Evaluation of climate models using palaeoclimatic data. *Nature Climate Change*, *2*(6), 417–424. https://doi.org/10.1038/nclimate1456

Braconnot, P., Otto-Bliesner, B., Harrison, S., Joussaume, S., Peterchmitt, J.-Y., Abe-Ouchi, A., et al. (2007). Results of PMIP2 coupled simulations of the Mid-Holocene and Last Glacial Maximum–Part 1: Experiments and large-scale features. *Climate of the Past*, *3*(2), 261–277. https://doi.org/10.5194/cp-3-261-2007

Brinkop, S., & Roeckner, E. (1995). Sensitivity of a general circulation model to parameterizations of cloud–turbulence interactions in the atmospheric boundary layer. *Tellus*, *47*(2), 197–220. https://doi.org/10.1034/j.1600-0870.1995.t01-1-00004.x

Buizert, C., Fudge, T. J., Roberts, W., Ritz, C., Lefebvre, E., Sherriff-Tadano, S., et al. (2019). How cold was Antarctica during the Last Glacial Maximum? In *Presented at the AGU fall meeting abstracts*, (Vol. *2019*, p. C13B-04).

Cao, J., Wang, B., & Liu, J. (2019). Attribution of the Last Glacial Maximum climate formation. *Climate Dynamics*, *53*(3), 1661–1679. https://doi.org/10.1007/s00382-019-04711-6

CLIMAP Project Members. (1976). The surface of the ice-age Earth. *Science*, *191*(4232), 1131–1137. https://doi.org/10.1126/science.191.4232.1131

Durack, P. J., & Taylor, K. E. (2019). input4MIPs.CMIP6.CMIP.PCMDI.PCMDI-AMIP-1-1-6 [Dataset]. Earth System Grid Federation. https://doi.org/10.22033/ESGF/input4MIPs.12381

Farrera, I., Harrison, S., Prentice, I., Ramstein, G., Joel, G., Bartlein, P., et al. (1999). Tropical climates at the Last Glacial Maximum: A new synthesis of terrestrial palaeoclimate data. I. Vegetation, lake-levels and geochemistry. *Climate Dynamics*, *15*(11), 823–856. https://doi.org/10.1007/s003820050317

Gates, W. L., Boyle, J. S., Covey, C., Dease, C. G., Doutriaux, C. M., Drach, R. S., et al. (1999). An overview of the results of the Atmospheric Model Intercomparison Project (AMIP I). *Bulletin of the American Meteorological Society*, *80*(1), 29–56. https://doi.org/10.1175/1520-0477(1999)080<0029:AOOTRO>2.0.CO;2

Hagemann, S., & Stacke, T. (2015). Impact of the soil hydrology scheme on simulated soil moisture memory. *Climate Dynamics*, *44*(7), 1731–1750. https://doi.org/10.1007/s00382-014-2221-6

Hargreaves, J., Annan, J., Yoshimori, M., & Abe-Ouchi, A. (2012). Can the Last Glacial Maximum constrain climate sensitivity? *Geophysical Research Letters*, *39*(24), 24702. https://doi.org/10.1029/2012GL053872

Hoffert, M. I., & Covey, C. (1992). Deriving global climate sensitivity from palaeoclimate reconstructions. *Nature*, *360*(6404), 573–576. https://doi.org/10.1038/360573a0

Kageyama, M., Albani, S., Braconnot, P., Harrison, S. P., Hopcroft, P. O., Ivanovic, R. F., et al. (2017). The PMIP4 contribution to CMIP6–Part 4: Scientific objectives and experimental design of the PMIP4-CMIP6 Last Glacial Maximum experiments and PMIP4 sensitivity experiments. *Geoscientific Model Development*, *10*(11), 4035–4055. https://doi.org/10.5194/gmd-10-4035-2017

Kageyama, M., Harrison, S. P., Kapsch, M.-L., Lofverstrom, M., Lora, J. M., Mikolajewicz, U., et al. (2021). The PMIP4 Last Glacial Maximum experiments: Preliminary results and comparison with the PMIP3 simulations. *Climate of the Past*, *17*(3), 1065–1089. https://doi.org/10.5194/cp-17-1065-2021

Krätschmer, S., van der Does, M., Lamy, F., Lohmann, G., Voelker, C., & Werner, M. (2022). Simulating glacial dust changes in the Southern Hemisphere using ECHAM6.3-HAM2.3. *Climate of the Past*, *18*(1), 67–87. https://doi.org/10.5194/cp-18-67-2022

Kurahashi-Nakamura, T., Paul, A., & Losch, M. (2017). Dynamical reconstruction of the global ocean state during the Last Glacial Maximum. *Paleoceanography*, *32*(4), 326–350. https://doi.org/10.1002/2016PA003001

Lamarque, J.-F., Bond, T. C., Eyring, V., Granier, C., Heil, A., Klimont, Z., et al. (2010). Historical (1850–2000) gridded anthropogenic and biomass burning emissions of reactive gases and aerosols: Methodology and application. *Atmospheric Chemistry and Physics*, *10*(15), 7017–7039. https://doi.org/10.5194/acp-10-7017-2010

Lin, S.-J., & Rood, R. (1996). Multidimensional flux-form semi-Lagrangian transport schemes. *Monthly Weather Review*, *124*(9), 2046–2070. https://doi.org/10.1175/1520-0493(1996)124<2046:MFFSLT>2.0.CO;2

Lohmann, G. (2020). Temperatures from energy balance models: The effective heat capacity matters. *Earth System Dynamics*, *11*(4), 1195–1208. https://doi.org/10.5194/esd-11-1195-2020

Lohmann, G., & Lorenz, S. (2000). On the hydrological cycle under paleoclimatic conditions as derived from AGCM simulations. *Journal of Geophysical Research*, *105*(D13), 17417–17436. https://doi.org/10.1029/2000JD900189

Lohmann, G., Wagner, A., & Prange, M. (2021). Resolution of the atmospheric model matters for the Northern Hemisphere Mid-Holocene climate. *Dynamics of Atmospheres and Oceans*, *93*, 101206. https://doi.org/10.1016/j.dynatmoce.2021.101206

Lohmann, U., & Roeckner, E. (1996). Design and performance of a new cloud microphysics scheme developed for the ECHAM general circulation model. *Climate Dynamics*, *12*(8), 557–572. https://doi.org/10.1007/BF00207939

Loomis, S. E., Russell, J. M., Verschuren, D., Morrill, C., De Cort, G., Sinninghe Damsté, J. S., et al. (2017). The tropical lapse rate steepened during the Last Glacial Maximum. *Science Advances*, *3*(1), e1600815. https://doi.org/10.1126/sciadv.1600815

Lott, F. (1999). Alleviation of stationary biases in a GCM through a mountain drag parameterization scheme and a simple representation of mountain lift forces. *Monthly Weather Review*, *127*(5), 788–801. https://doi.org/10.1175/1520-0493(1999)127<0788:AOSBIA>2.0.CO;2

Meehl, G. A., Senior, C. A., Eyring, V., Flato, G., Lamarque, J.-F., Stouffer, R. J., et al. (2020). Context for interpreting equilibrium climate sensitivity and transient climate response from the CMIP6 Earth system models. *Science Advances*, *6*(26), eaba1981. https://doi.org/10.1126/sciadv.aba1981

Meyer, V. D., Hefter, J., Lohmann, G., Max, L., Tiedemann, R., & Mollenhauer, G. (2017). Summer temperature evolution on the Kamchatka Peninsula, Russian far East, during the past 20,000 years. *Climate of the Past*, *13*(4), 359–377. https://doi.org/10.5194/cp-13-359-2017

Mix, A., Morey, A., Pisias, N., & Hostetler, S. (1999). Foraminiferal faunal estimates of paleotemperature: Circumventing the no-analog problem yields cool ice age tropics. *Paleoceanography*, *14*(3), 350–359. https://doi.org/10.1029/1999PA900012

Neubauer, D., Ferrachat, S., Siegenthaler-Le Drian, C., Stier, P., Partridge, D. G., Tegen, I., et al. (2019). The global aerosol–climate model ECHAM6.3–HAM2.3–Part 2: Cloud evaluation, aerosol radiative forcing, and climate sensitivity. *Geoscientific Model Development*, *12*(8), 3609–3639. https://doi.org/10.5194/gmd-12-3609-2019

Otto, J., Raddatz, T., & Claussen, M. (2011). Strength of forest-albedo feedback in Mid-Holocene climate simulations. *Climate of the Past*, *7*(3), 1027–1039. https://doi.org/10.5194/cp-7-1027-2011

Paul, A., Mulitza, S., Stein, R., & Werner, M. (2021). A global climatology of the ocean surface during the Last Glacial Maximum mapped on a regular grid (GLOMAP). *Climate of the Past*, *17*(2), 805–824. https://doi.org/10.5194/cp-17-805-2021

Paul, A., & Schäfer-Neth, C. (2003). Modeling the water masses of the Atlantic Ocean at the Last Glacial Maximum. *Paleoceanography*, *18*(3), 1058. https://doi.org/10.1029/2002PA000783

Powers, L., Johnson, T. C., Werne, J., Castañeda, I., Ec, H., Sinninghe-Damste, J., & Schouten, S. (2005). Large temperature variability in the southern African tropics since the Last Glacial Maximum. *Geophysical Research Letters*, *32*(8), L08706. https://doi.org/10.1029/2004GL022014

Reick, C. H., Raddatz, T., Brovkin, V., & Gayler, V. (2013). Representation of natural and anthropogenic land cover change in MPI-ESM. *Journal of Advances in Modeling Earth Systems*, *5*(3), 459–482. https://doi.org/10.1002/jame.20022

Roeckner, E., Brokopf, R., Esch, M., Giorgetta, M., Hagemann, S., Kornblueh, L., et al. (2006). Sensitivity of simulated climate to horizontal and vertical resolution in the ECHAM5 atmosphere model. *Journal of Climate*, *19*(16), 3771–3791. https://doi.org/10.1175/JCLI3824.1

Romanova, V., Lohmann, G., Grosfeld, K., & Butzin, M. (2006). The relative role of oceanic heat transport and orography on glacial climate. *Quaternary Science Reviews*, *25*(7), 832–845. https://doi.org/10.1016/j.quascirev.2005.07.007

Schmittner, A., Urban, N. M., Shakun, J. D., Mahowald, N. M., Clark, P. U., Bartlein, P. J., et al. (2011). Climate sensitivity estimated from temperature reconstructions of the Last Glacial Maximum. *Science*, *334*(6061), 1385–1388. https://doi.org/10.1126/science.1203513

Schneider von Deimling, T., Ganopolski, A., Held, H., & Rahmstorf, S. (2006). How cold was the Last Glacial Maximum? *Geophysical Research Letters*, *33*(14), L14709. https://doi.org/10.1029/2006GL026484

Seltzer, A. M., Ng, J., Aeschbach, W., Kipfer, R., Kulongoski, J. T., Severinghaus, J. P., & Stute, M. (2021). Widespread six degrees celsius cooling on land during the Last Glacial Maximum. *Nature*, *593*(7858), 228–232. https://doi.org/10.1038/s41586-021-03467-6

Simmons, A. J., Burridge, D. M., Jarraud, M., Girard, C., & Wergen, W. (1989). The ECMWF medium-range prediction models development of the numerical formulations and the impact of increased resolution. *Meteorology and Atmospheric Physics*, *40*(1), 28–60. https://doi.org/10.1007/BF01027467

Simmons, A. J., & Jiabin, C. (1991). The calculation of geopotential and the pressure gradient in the ECMWF atmospheric model: Influence on the simulation of the polar atmosphere and on temperature analyses. *Quarterly Journal of the Royal Meteorological Society*, *117*(497), 29–58. https://doi.org/10.1002/qj.49711749703

Stärz, M., Lohmann, G., & Knorr, G. (2016). The effect of a dynamic soil scheme on the climate of the Mid-Holocene and the Last Glacial Maximum. *Climate of the Past*, *12*(1), 151–170. https://doi.org/10.5194/cp-12-151-2016

Stevens, B., Giorgetta, M., Esch, M., Mauritsen, T., Crueger, T., Rast, S., et al. (2013). Atmospheric component of the MPI-M Earth system model: ECHAM6: ECHAM6. *Journal of Advances in Modeling Earth Systems*, *5*(2), 146–172. https://doi.org/10.1002/jame.20015

Stier, P., Feichter, J., Kinne, S., Kloster, S., Vignati, E., Wilson, J., et al. (2005). The aerosol-climate model ECHAM5-HAM. *Atmospheric Chemistry and Physics*, *5*(4), 1125–1156. https://doi.org/10.5194/acp-5-1125-2005

Sundqvist, H., Berge, E., & Kristjánsson, J. E. (1989). Condensation and cloud parameterization studies with a mesoscale numerical weather prediction model. *Monthly Weather Review*, *117*(8), 1641–1657. https://doi.org/10.1175/1520-0493(1989)117<1641:CACPSW>2.0.CO;2

Tarasov, L., Dyke, A., Neal, R., & Peltier, W. (2012). A data-calibrated distribution of deglacial chronologies for the North American ice complex from glaciological modeling. *Earth and Planetary Science Letters*, *315*, 30–40. https://doi.org/10.1016/j.epsl.2011.09.010

Tegen, I., Neubauer, D., Ferrachat, S., Siegenthaler-Le Drian, C., Bey, I., Schutgens, N., et al. (2019). The global aerosol–climate model ECHAM6.3–HAM2.3–Part 1: Aerosol evaluation. *Geoscientific Model Development*, *12*(4), 1643–1677. https://doi.org/10.5194/gmd-12-1643-2019

Tierney, J. E., Zhu, J., King, J., Malevich, S. B., Hakim, G. J., & Poulsen, C. J. (2020). Glacial cooling and climate sensitivity revisited. *Nature*, *584*(7822), 569–573. https://doi.org/10.1038/s41586-020-2617-x

Waelbroeck, C., Paul, A., Kucera, M., Rosell-Melé, A., Weinelt, M., Schneider, R., et al. (2009). Constraints on the magnitude and patterns of ocean cooling at the Last Glacial Maximum. *Nature Geoscience*, *2*(2), 127–132. https://doi.org/10.1038/ngeo411

Wang, R., Kuhn, G., Gong, X., Biskaborn, B., Gersonde, R., Lembke-Jene, L., et al. (2021). Deglacial land-ocean linkages at the Alaskan continental margin in the Bering Sea. *Frontiers of Earth Science*, *9*, 1. https://doi.org/10.3389/feart.2021.712415

Yin, J. H., & Battisti, D. S. (2001). The importance of tropical sea surface temperature patterns in simulations of Last Glacial Maximum climate. *Journal of Climate*, *14*(4), 565–581. https://doi.org/10.1175/1520-0442(2001)014<0565:TIOTSS>2.0.CO;2